# Population-Based Evaluation of Retinal Nerve Fiber Layer, Retinal Ganglion Cell Layer, and Inner Plexiform Layer as a Diagnostic Tool For Glaucoma

Henriët Springelkamp,[1,2] Kyungmoo Lee,[3] Roger C. W. Wolfs,[1] Gabriëlle H. S. Buitendijk,[1,2] Wishal D. Ramdas,[1,2] Albert Hofman,[2,4] Johannes R. Vingerling,[1,2] Caroline C. W. Klaver,[1,2] Michael D. Abràmoff,[3,5–7] and Nomdo M. Jansonius[2,8]

[1]Department of Ophthalmology, Erasmus Medical Center, Rotterdam, The Netherlands
[2]Department of Epidemiology, Erasmus Medical Center, Rotterdam, The Netherlands
[3]Department of Electrical and Computer Engineering, University of Iowa, Iowa City, Iowa, United States
[4]Netherlands Consortium for Healthy Ageing, Netherlands Genomics Initiative, The Hague, The Netherlands
[5]Department of Ophthalmology and Visual Sciences, University of Iowa, Iowa City, Iowa, United States
[6]Department of Biomedical Engineering, University of Iowa, Iowa City, Iowa, United States
[7]United States Department of Veterans Affairs, Iowa City, Iowa, United States
[8]Department of Ophthalmology, University of Groningen, University Medical Center Groningen, Groningen, The Netherlands

Correspondence: Michael D. Abràmoff, Department of Ophthalmology and Visual Sciences 11205 PFP, University of Iowa Hospitals and Clinics, Iowa City, IA 52242; michael-abramoff@uiowa.edu.

Submitted: August 19, 2014
Accepted: October 30, 2014

Citation: Springelkamp H, Lee K, Wolfs RCW, et al. Population-based evaluation of retinal nerve fiber layer, retinal ganglion cell layer, and inner plexiform layer as a diagnostic tool for glaucoma. *Invest Ophthalmol Vis Sci.* 2014;55:8428–8438. DOI:10.1167/iovs.14-15506

**Purpose.** We determined the glaucoma screening performance of regional optical coherence tomography (OCT) layer thickness measurements in the peripapillary and macular region, in a population-based setting.

**Methods.** Subjects ($n$ = 1224) in the Rotterdam Study underwent visual field testing (Humphrey Field Analyzer) and OCT of the macula and optic nerve head (Topcon 3-D OCT-1000). We determined the mean thicknesses of the retinal nerve fiber layer (RNFL), retinal ganglion cell layer (RGCL), and inner plexiform layer for regions-of-interest; thus, defining a series of OCT parameters, using the Iowa Reference Algorithms. Reference standard was the presence of glaucomatous visual field loss (GVFL); controls were subjects without GVFL, an intraocular pressure (IOP) of 21 mm Hg or less, and no positive family history for glaucoma. We calculated the area under the receiver operating characteristics curve (AUCs) and the sensitivity at 97.5% specificity for each parameter.

**Results.** After excluding 23 subjects with an IOP > 21 mm Hg and 73 subjects with a positive family history for glaucoma, there were 1087 controls and 41 glaucoma cases. Mean RGCL thickness in the inferior half of the macular region showed the highest AUC (0.85; 95% confidence interval [CI] 0.77–0.92) and sensitivity (53.7%; 95% CI, 38.7–68.0%). The mean thickness of the peripapillary RNFL had an AUC of 0.77 (95% CI, 0.69–0.85) and a sensitivity of 24.4% (95% CI, 13.7–39.5%).

**Conclusions.** Macular RGCL loss is at least as common as peripapillary RNFL abnormalities in population-based glaucoma cases. Screening for glaucoma using OCT-derived regional thickness identifies approximately half of those cases of glaucoma as diagnosed by perimetry.

Keywords: OCT, retinal thickness measurement, Iowa Reference Algorithms, population-based evaluation

Glaucoma is a chronic optic neuropathy with associated damage of retinal ganglion cells, which results in visual field loss. This damage is characterized by increased cupping of the optic nerve head (ONH), and thinning of the retinal nerve fiber layer (RNFL) and retinal ganglion cell layer (RGCL), as has been shown with fundus photography, histology, and optical coherence tomography (OCT).[1–3] These structures can be assessed with the Heidelberg Retina Tomograph (HRT; Heidelberg Engineering, Dossenheim, Germany)[4] or with scanning laser polarimetry (GDx Nerve Fiber Analyzer; Carl Zeiss Meditec, Jena, Germany).[5,6] These techniques showed an apparently favorable screening performance in some specific study populations.[7,8] In population-based settings, however, the screening performance of these techniques was rather poor.[9–12] A good screening performance in population-based settings is indispensable for an effective case finding for population-based glaucoma research.

The OCT is a newer technique, which can quantify volumes of different retinal layers through segmentation and detect glaucomatous changes of retina and ONH.[3,13] Similar to what was found in HRT and GDx, many studies reported a favorable screening performance of OCT in clinical settings. Thus far, only two studies were designed as population-based studies, with relatively small sample sizes and, as a consequence, a very small number of cases (9 cases[14] and 6 cases,[15] respectively). Population-based studies are attractive, compared to clinical studies, because of the absence of selection bias.

The aim of this study was to determine, in a population-based setting, the glaucoma screening performance of OCT combined with fully 3D analysis, with glaucomatous visual field loss (GVFL) as the reference standard. Specifically, we evaluated the following metrics: peripapillary RNFL thickness, macular mean RGCL, RNFL, and inner plexiform layer (IPL) thicknesses, and mean RGCL, RNFL, and IPL thicknesses in regions based on the trajectories of the nerve fiber bundles and the macular vulnerability zone.[16–20]

## Methods

### Study Population

The Rotterdam Study is a prospective cohort study investigating age-related disorders.[21] It is conducted in Rotterdam, The Netherlands. It started in 1990 with the original cohort, which comprised 7983 subjects aged 55 years or older. The study was enlarged with two additional cohorts in 2000 (3011 subjects aged 55 years or older) and 2006 (3932 subjects aged 45 years or older). Follow-up examinations still are ongoing. The ophthalmic examinations have been described previously.[22] All measurements were conducted after the Medical Ethics Committee of the Erasmus Medical Center had approved the study protocol and after all subjects had provided written informed consent in accordance with the tenets of the Declaration of Helsinki.

### Cases and Controls

We included 1224 consecutive subjects from the third Rotterdam Study cohort (baseline examinations) and the original Rotterdam Study cohort (fourth follow-up examinations) who had undergone intraocular pressure (IOP) measurement, perimetry, and spectral domain OCT (see below). After this consecutive inclusion, we continued to include subjects with GVFL to circumvent the low prevalence of glaucoma. Subjects with GVFL (see below) in at least one eye were considered cases, irrespective of their IOP. Subjects without GVFL, an IOP of 21 mm Hg or less, and no positive family history for glaucoma were considered controls. If both eyes were eligible, we used data from a random eye. If GVFL was present in one eye, we used data from the eye with GVFL. Due to the extended inclusion of cases, which took place in a younger cohort, the cases and controls were incidentally almost perfectly age-matched (see Results section), even though a difference in age would have been expected.[23]

### Visual Field Testing

All subjects in the present study were tested for visual field defects using the Humphrey Field Analyzer (HFA; Carl Zeiss Meditec, Jena, Germany). Details of this assessment have been published previously.[23] Briefly, each eye was screened using a 52-point supra-threshold test that covered the central visual field with a radius of 24°. If the subject did not respond to the light stimulus (6 dB above a threshold-related estimate of the hill of vision) in at least three contiguous test points (or four including the blind spot) in two supra-threshold tests, full-threshold HFA testing with a 24-2 grid was performed. The full-threshold tests were classified as abnormal if at least one of three criteria was met: (1) a Glaucoma Hemifield Test "outside normal limits," (2) a minimum of three contiguous points in the pattern deviation probability plot with a sensitivity decreased to $P < 0.05$ of which at least one point to $P < 0.01$, or (3) a Pattern Standard Deviation $P < 5\%$. Visual field loss was considered to be present if it was reproducible, that is, the abnormalities had to be present on the full-threshold test and on both supra-threshold tests. Defects had to be in the same hemifield and at least one depressed test point had to have exactly the same location on all fields. Fundus photographs, ophthalmic examination reports, medical histories, and MRI scans of the brain were checked for disorders that could explain the visual field loss. If no other cause could be identified, and no homonymous defects and artifacts like rim artifacts were found, the visual field loss was considered GVFL. Discrepancies were resolved by consensus.

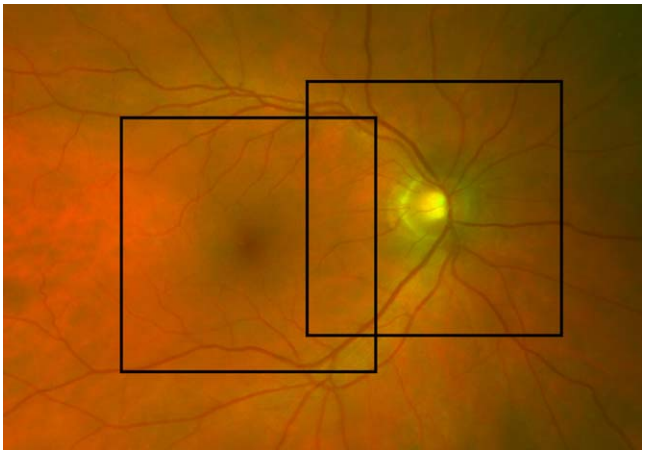

Figure 1. Schematic overview of the area of the macular scan (*left square*) and ONH scan (*right square*).

### Optic Disc Assessment

Subjects underwent optic disc assessment using the HRT device. The cutoff values for glaucomatous optic neuropathy (GON) were based on the linear cup-disc ratio (LCDR) and defined as follows: 0.67 for small discs (up to 1.5 $mm^2$), 0.71 for discs 1.5 to 2.0 $mm^2$, and 0.76 for large discs (>2.0 $mm^2$).[10] We excluded HRT scans that exceeded a SD of 50 μm.

### Optical Coherence Tomography (OCT)

Since 2007, the macula and ONH of all visiting subjects have been imaged with OCT (Topcon 3-D OCT-1000; Topcon, Tokyo, Japan). At the beginning of the study, only the right eye was scanned in the interest of time. We included $n = 883$ subjects during this period. In a later stage, both eyes were scanned. Due to an update during the study, seven glaucoma cases were scanned with the Topcon OCT-2000 instead of the OCT-1000 (the inclusion of cases was extended because of the low prevalence of GVFL, see above). Importantly, the segmentation algorithm corrects for differences between these two devices. To confirm this, we excluded these seven cases and reanalyzed the data (see Results section). Macular and ONH scans were centered around the fovea and the center of the ONH, respectively. Figure 1 shows the scanned areas. The scans were performed in the horizontal direction. Volume size was $6 \times 6 \times 1.68$ mm ($512 \times 128 \times 480$ voxels). Volumes with severe motion artifacts caused by head or eye movements and macular volumes in which more than 20% of the volume was unsegmentable were excluded. The ONH volumes with one or more clock hour segments (see below) in which the RNFL was completely unsegmentable also were excluded. All included OCT volumes were segmented into 10 layers (11 surfaces), using the Iowa Reference Algorithms (available in the public domain from http://biomed-imaging.uiowa.edu/downloads), a fully three-dimensional automated segmentation algorithm.[24–26] We studied the RNFL (between surfaces 1 and 2),

Investigative Ophthalmology & Visual Science

Table 1. Overview of the Included OCT Parameters

| Region | Parameter | Layer | Measure* |
|---|---|---|---|
| ONH | Mean thickness (μm) in peripapillary region | RNFL | Continuous |
| | Number of abnormally thin subregions; subregions are peripapillary 30° segments with the 4 nasal segments combined | RNFL | Score 0–9 |
| Macula | Mean thickness (μm) in scan region | RGCL<br>RGCL + RNFL<br>RGCL + RNFL + IPL | Continuous |
| | Number of abnormally thin subregions; 11 subregions as presented in Figure 2A | RGCL<br>RGCL + RNFL<br>RGCL + RNFL + IPL | Score 0–11 |
| | Number of abnormally thin subregions; 4 subregions as presented in Figure 2B | RGCL<br>RGCL + RNFL<br>RGCL + RNFL + IPL | Score 0–4 |
| | Mean thickness in MVZ (μm, Fig. 2C) | RGCL<br>RGCL + RNFL<br>RGCL + RNFL + IPL | Continuous |
| | Mean thickness in inferior half of macular scan (μm) | RGCL<br>RGCL + RNFL<br>RGCL + RNFL + IPL | Continuous |
| Combined | 11 macular subregions (Fig. 2A) with weight factor 4/11 combined with 5 ONH subregions: 2 superior 30° segments, 2 inferior 30° segments, and 1 nasal 120° segment | | Score 0–9 |
| | 4 macular subregions (Fig. 2B) combined with 5 ONH subregions: 2 superior 30° segments, 2 inferior 30° segments, and 1 nasal 120° segment | | Score 0–9 |

* Continuous variable or number of subregions with a thickness below a certain percentile.

the RGCL (between surfaces 2 and 3), and the IPL (between surfaces 3 and 4). For the macula, we calculated the thicknesses of these layers in 100 square blocks of 0.6 × 0.6 mm each. For the ONH, we calculated the thickness of the RNFL in between two circles with radii of 1.03 and 1.84 mm centered on the manually determined ONH center.[27] This was done in 12 peripapillary segments of 30° each (one clock hour).

## Data Analysis

We calculated the area under the receiver operating characteristics Curves (AUC) for different parameters. Starting with the 100 blocks from the macular region and the 12 peripapillary segments, we constructed a series of parameters. These parameters comprised global measures and more detailed measures, based on the pathophysiology of glaucoma. We used the retinal nerve fiber bundle trajectories as described by Jansonius et al.[18,19] to divide the macular area in 11 subregions. As this subdivision might be too fine-grained given the test–retest variability of OCT measurements,[27] we divided the macular area in 4 larger scale subregions as well. We focused on a specific region of the macula, the macular vulnerability zone (MVZ)[17] and—related to the MVZ—the inferior half of the macular scan. Table 1 lists all included parameters; Figure 2 presents the 11 and 4 subregions based on the trajectories, and the MVZ.

For AUC analysis, a single variable is needed. For the global measures, there is only one region-of-interest and, thus, the average thickness of a particular layer in that region is a single variable. For the measures based on a number of subregions, we made a single variable (a score) by counting the number of subregions that had a thickness of a particular layer below a certain percentile. This was repeated for a series of percentiles (P0.5, P1, P2, P5, P10, P20; based on the controls). The percentile yielding the highest AUC was selected. Analyses concerning the macular region were done for the RGCL, and unweighted summations of RGCL + RNFL, and RGCL + RNFL + IPL. Analyses concerning the ONH region were based on the RNFL. The 95% percent confidence intervals (95% CI) were calculated and the highest AUCs from the macula and ONH were compared using a technique described by DeLong et al.[28] We performed a cross-validation by calculating an adjusted AUC of the parameter with the highest (uncorrected) AUC and sensitivity using a leave-one-out resampling method.

We calculated the sensitivity at a fixed high specificity of 97.5% for all included parameters, for the best percentile/layer combination, if applicable.[29] Sensitivities were compared with a McNemar test. For the parameter with the highest AUC and highest sensitivity, the positive and negative predictive values were calculated. For these parameters, we also calculated the sensitivity and AUC for glaucoma defined as HRT-based GON (see above) and as the presence of GON and GVFL. Analyses were performed with IBM SPSS Statistics Release 21.0.0.1 (IBM Corp., Armonk, NY, USA). The comparisons of AUCs were performed using MedCalc Statistical Software version 12.7.7 (MedCalc Software bvba, Ostend, Belgium; available in the public domain at http://www.medcalc.org; 2013). The leave-one-out cross-validation was performed using R version 3.0.2 (cvAUC package; R Foundation for Statistical Computing, Vienna, Austria; available in the public domain at http://www.R-project.org/; 2013). A $P$ value below 0.05 was considered statistically significant.

## Results

We excluded 23 controls with an IOP > 21 mm Hg and 73 controls with a positive family history for glaucoma. After this, there were 1128 subjects left: 1087 controls and 41 GVFL cases. Controls and cases did not differ in age (74.8 vs. 74.2 years, $P = 0.66$) or sex (40.6 vs. 41.5% male, $P = 0.91$). The average (median) mean deviation (MD) of the visual field of the cases was −7.5 (−6.5) dB (SD, −4.9 dB; interquartile range, −3.8 to −10.5 dB).

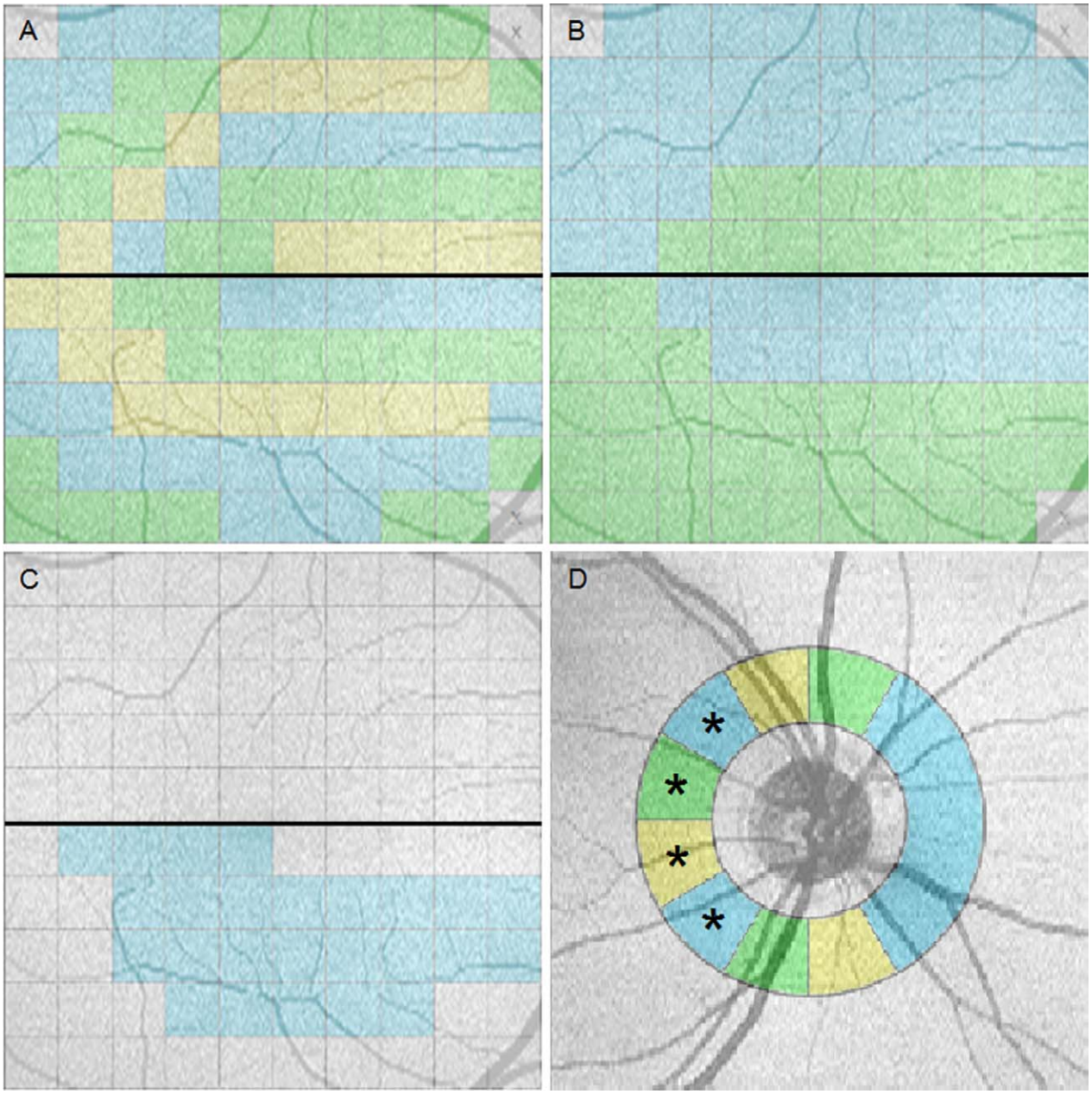


FIGURE 2. Division of macular scan region in 11 (**A**) and 4 (**B**) color-coded subregions, based on the nerve fiber bundle trajectories as described by Jansonius et al.,[18,19] and the MVZ (**C**) as described by Hood et al.[17] *Dark line* represents the border between the superior and inferior part of the scan. Division of peripapillary region in 9 color-coded segments ([**D**]; *denotes segments that are replaced by macular subregions in the combined variables as described in Table 1).

Table 2 shows the AUCs for the different OCT parameters. None of the parameters had a higher AUC than the mean RGCL thickness in the entire macular region (0.85; 95% CI, 0.78–0.93). A more detailed analysis did not improve the AUC (0.85 for 11 bundles), nor did confining the analysis to the inferior half of the macular region (0.85). Including additional retinal layers to the thickness measurements (RGCL + RNFL or RGCL + RNFL + IPL), acceptable from an anatomical perspective, yielded lower AUC point estimates. The average RNFL thickness in the ONH volume yielded an AUC of 0.77 (95% CI, 0.69–0.85; significantly lower than that of the mean RGCL thickness in the entire macular region; $P = 0.01$); a detailed analysis of 9 peripapillary segments resulted in essentially the same AUC (0.78). Combined analysis of macular bundles and peripapillary segments did not yield any diagnostic improvement.

Table 3 shows the sensitivity at an approximately 97.5% specificity level for the layer and/or percentile with the highest AUC for each OCT parameter. The mean RGCL thickness in the inferior half of the macular region had the highest sensitivity (53.7%; 95% CI, 38.7–68.0%) followed by the mean RGCL thickness in the MVZ (46.3%; 95% CI, 32.1–61.3%). The positive and negative predictive values of the former parameter were 44.9% and 98.2%, respectively. The difference between these two sensitivities was not significant ($P = 0.25$). The mean peripapillary RNFL thickness had a sensitivity of 24.4% (95% CI, 13.7–39.5%; $P < 0.001$ compared to the mean RGCL thickness in inferior half of the macular region). The corrected

**Table 2.** AUCs for the OCT Parameters as Listed in Table 1

| Region | Parameters | Layer | AUC | | | | | |
|---|---|---|---|---|---|---|---|---|
| | | | P0.5 | P1 | P2 | P5 | P10 | P20 |
| ONH | Mean of all segments | RNFL | | | 0.77 | | | |
| | Score based on 9 segments | RNFL | 0.57 | 0.64 | 0.66 | 0.76 | 0.78 | 0.76 |
| Macula | Mean in whole scan | RGCL | | | 0.85 | | | |
| | | RNFL + RGCL | | | 0.83 | | | |
| | | RNFL + RGCL + IPL | | | 0.78 | | | |
| | Score based on 11 bundles | RGCL | 0.68 | 0.80 | 0.82 | 0.85 | 0.83 | 0.84 |
| | | RNFL + RGCL | 0.67 | 0.76 | 0.82 | 0.84 | 0.84 | 0.82 |
| | | RNFL + RGCL + IPL | 0.64 | 0.71 | 0.77 | 0.81 | 0.81 | 0.78 |
| | Score based on 4 bundles | RGCL | 0.60 | 0.71 | 0.78 | 0.83 | 0.83 | 0.84 |
| | | RNFL + RGCL | 0.65 | 0.68 | 0.78 | 0.80 | 0.82 | 0.81 |
| | | RNFL + RGCL + IPL | 0.57 | 0.65 | 0.73 | 0.79 | 0.79 | 0.76 |
| | Mean in MVZ | RGCL | | | 0.83 | | | |
| | | RNFL + RGCL | | | 0.79 | | | |
| | | RNFL + RGCL + IPL | | | 0.78 | | | |
| | Mean in inferior scan | RGCL | | | 0.85 | | | |
| | | RNFL + RGCL | | | 0.81 | | | |
| | | RNFL + RGCL + IPL | | | 0.79 | | | |
| Combined | Score based on ONH RNFL (P10) + 11 macular bundles RGCL (P5) | | | | 0.85 | | | |
| | Score based on ONH RNFL (P10) + 4 macular bundles RGCL (P20) | | | | 0.85 | | | |

P0.5, P1, P2, P5, P10, and P20 are percentiles based on the controls in this study population that are used as cutoff values to calculated the scores (see Table 1).

AUC for the parameter with the highest AUC and sensitivity (mean RGCL thickness in the inferior half of the macular region; AUC = 0.85) was 0.84 (leave-one-out cross-validation). No significant differences were found for this parameter after exclusion of the subjects who were scanned with the OCT-2000: AUC and sensitivity at 97.5% specificity were 0.83 and 52.9%, respectively.

Of the 41 cases, 19 were not identified by "mean RGCL thickness in the inferior half of the macular region." Figure 3 shows the MD and pattern standard deviation (PSD) values of the 41 cases, stratified according to true-positive and false-negative status. The MD and PSD values of the 19 false-negatives seemed to be higher and lower, respectively, than that of the 22 true-positives, but the differences were not significant (MD, –6.2 vs. –8.6 dB, $P = 0.13$; PSD, 7.1 vs. 9.0 dB, $P = 0.09$). Figure 4 presents the mean sensitivity in the superior half of the visual field (8 superiorly located central test locations of 24-2 grid) as a function of the mean RGCL thickness in the inferior half of the macular scan, for the 41 cases with GVFL. There was a significant association ($R = 0.35$, $P = 0.026$). True-positives had on average a lower threshold sensitivity in the central part of the superior visual field compared to false-negatives (19.6 vs. 24.7 dB, $P = 0.042$). There was no difference in axial length between cases and controls (23.8 vs. 23.5 mm, $P = 0.09$; based on 33 cases and 903 controls for which axial length data were available), but true-positives had a greater axial length than false-negatives (24.1 vs. 23.4 mm, $P = 0.049$). Finally, Figure 5 presents the mean superior macular thickness versus the mean inferior macular thickness for the RGCL, for cases and controls.

Table 4 shows the sensitivity at 97.5% specificity and AUC for patients with HRT-based GON ($n = 37$), and GON and GVFL ($n = 10$). The sensitivity and AUC of the "mean RGCL thickness in the inferior half of the macular region" increased from 53.7% to 70.0% and from 0.85 to 0.93, respectively, for cases with GON and GVFL.

**Table 3.** Sensitivity, at 97.5% Specificity, for the Layers and Percentiles With the Best AUC (Table 2)

| Region | Variable | % Specificity* | % Sensitivity |
|---|---|---|---|
| ONH | Mean RNFL of all segments | 97.5 | 24.4 |
| | RNFL score: P10 | 96.1 | 29.3 |
| | | 98.0 | 14.6 |
| Macula | Mean of whole scan, RGCL | 97.5 | 36.6 |
| | 11 bundles, RGCL P5 | 97.2 | 29.3 |
| | | 98.1 | 29.3 |
| | 4 bundles, RGCL P20 | 93.8† | 41.5 |
| | Mean of MVZ, RGCL | 97.5 | 46.3 |
| | Mean of inferior scan, RGCL | 97.5 | 53.7 |
| Combined | ONH RNFL P10 + 4 bundles RGCL P20 | 97.0 | 31.7 |
| | | 98.1 | 22.0 |
| | ONH RNFL P10 + 11 bundles RGCL P5 | 97.5 | 26.8 |

* If none of the cutoff points yielded a specificity of exactly 97.5%, two specificity values were reported that enclose 97.5%.
† Highest possible specificity for this parameter.

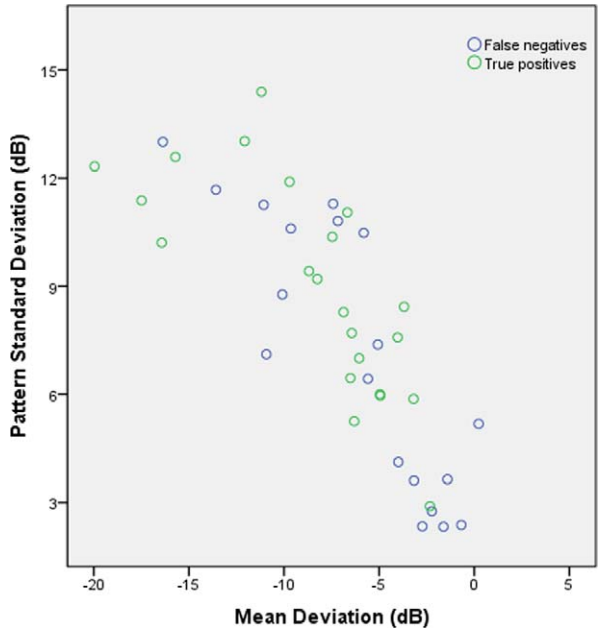


FIGURE 3. Scatterplot of mean deviation versus pattern SD for the 41 cases with GVFL. *Green dots* represent the cases ($n = 22$) correctly classified by the mean RGCL thickness in the inferior half of the macular region (true-positives). *Blue dots* represent the false-negative cases ($n = 19$).

## DISCUSSION

Our results showed that the mean RGCL thickness in the inferior half of the macular region has the best performance in terms of AUC and sensitivity at 97.5% specificity in this population-based OCT study. The sensitivity of 53.7% results in missing almost half of GFVL cases if OCT is applied for mass screening for glaucoma, as defined by our criteria of visual field loss.

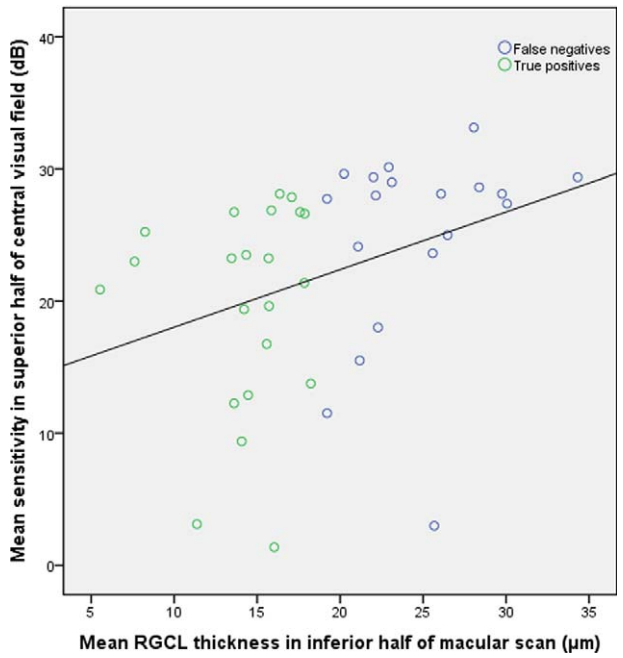


FIGURE 4. Scatterplot of the mean RGCL thickness in the inferior half of the macular scan versus the mean sensitivity of the eight superiorly located central test locations of the 24-2 grid for the 41 cases with GVFL.

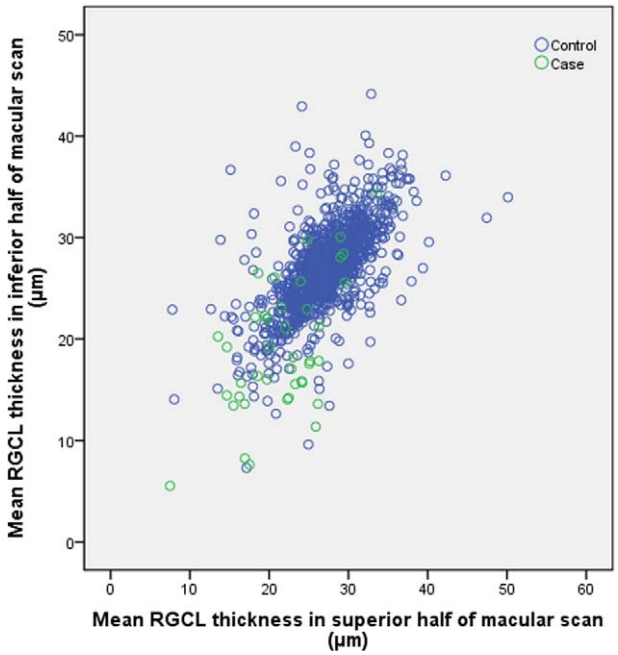


FIGURE 5. Mean superior macular thickness versus mean inferior macular thickness for the RGCL, for cases (*green*) and controls (*blue*).

The AUC is a commonly reported measure for the diagnostic performance of a test. It is a summary measure compiled from the sensitivity and specificity for a range of cut-off values. Given the low prevalence of glaucoma in a population, however, sensitivities at low specificities have diminished relevance. This makes sensitivity at a fixed high specificity a more relevant measure. Therefore, we consider "mean RGCL thickness in the inferior half of the macular region" the best parameter, despite the fact that many other parameters had comparable AUCs. The 97.5% specificity level has an optimal balance between false-positive and true-positive classification for risk factor analysis.[29] For screening as part of preventing a disease, the specificity also is a trade-off between yield and cost, and a different cutoff value may be preferred from either perspective. However, a cost-effectiveness analysis is not the purpose of this current study.

Recently, several studies focusing on glaucomatous macular damage have been published.[30–37] The macular ganglion cell complex (GCC; i.e., RNFL + RGCL + IPL) is on average thinner in glaucomatous eyes and correlates with visual field changes. Our study included mainly patients with early and moderate

TABLE 4. Sensitivity at 97.5% Specificity and AUC for Mean RGCL Thickness in the Inferior Half of the Macular Region and Mean RNFL Thickness in Peripapillary Region, for Cases With HRT-Based GON ($n = 37$), and Cases With GON and GVFL ($n = 10$)

| | GVFL | GON | GVFL and GON |
|---|---|---|---|
| Mean of macular inferior scan, RGCL | | | |
| Sensitivity | 53.7 | 24.3 | 70.0 |
| AUC | 0.85 | 0.71 | 0.93 |
| Mean RNFL of all peripapillary segments | | | |
| Sensitivity | 24.4 | 16.2 | 40.0 |
| AUC | 0.77 | 0.78 | 0.95 |

**Table 5.** Overview of Published Literature Regarding Glaucoma Screening With OCT

| Reference | Definition of Glaucoma | *N* of Cases | *N* of Controls | OCT Device | Parameter | Best Parameter(s) | % Sensitivity | % Specificity | AUC |
|---|---|---|---|---|---|---|---|---|---|
| Baskaran et al.[46] | GON + GVFD | 184 | 508 | Cirrus HD-OCT | RNFL: average, quadrant and clock-hours | Average | x | x | 0.92 |
| | | | | | | Inferior | x | x | 0.92 |
| | | | | | ONH | VCDR | x | x | 0.91 |
| Bengtsson et al.[14] | GON | 138 clinical cases | 129 healthy subjects from population | TD Stratus OCT | RNFL: average, quadrant and clock-hours | average <P5 | 78 | 99 | x |
| | | | | | | ≥1 quadrant sector <P5 | 93 | 93 | x |
| | | | | | | ≥1 clock hours <P5 | 95 | 81 | x |
| | | | | SD Cirrus OCT | RNFL: average, quadrant and clock-hours | Average <P5 | 90 | 95 | x |
| | | | | | | ≥1 quadrant sector <P5 | 96 | 81 | x |
| | | | | | | ≥1 clock-hours <P5 | 94 | 65 | x |
| Bowd et al.[48] | GON and/or GVFD | 156 | 69 | Stratus-OCT | RNFL: average, superior and inferior | Average | 58 | 90 | 0.78 |
| Garas et al.[42] | GON + GVFD | 111 | 93 | RTVue-100 FD OCT | RNFL: average, superior and inferior sectors, 16 segments | Infero-Temporal segment | 88.3 | 97.8 | x |
| | | | | | Macula: GCC | FLV | 92.8 | 89.1 | x |
| | | | | | ONH | Cup area or rim area (same results) | 85.6 | 76.3 | x |
| Huang et al.[43] | GVFD | 146 | 74 | RTVue OCT | RNFL: 8 segments | Average | 81.5 | 87.8 | 0.92 |
| | | | | | ONH | VCDR | 71.9 | 91.9 | 0.85 |
| | | | | | Macula: IRL | Inferior hemisphere thickness | 74.7 | 90.5 | 0.87 |
| Jeoung et al.[44] | GON + GVFD | 142 | 119 | Cirrus HD-OCT | RNFL: average, quadrant and clock-hours | Average | 83.1 | 96.6 | 0.96 |
| | | | | | | Inferior | 86.6 | 94.6 | 0.96 |
| | | | | | ONH | Rim area | 80.5 | 86.6 | 0.94 |
| | | | | | Macular GCIPL: average, minimal and 6 sectors | Minimal GCIPL | 90.8 | 88.2 | 0.96 |
| | | 164 | 119 | Cirrus HD-OCT | RNFL: idem | average | 50 | 96.6 | 0.90 |
| | | | | | ONH: idem | rim area | 61 | 86.6 | 0.86 |
| | | | | | Macular GCIPL: idem | minimal GCIPL | 73.2 | 88.2 | 0.90 |
| Leung et al.[49] | GVFD | 121 | 102 | TD Stratus OCT | RNFL: clock-hour, quadrant and average | ≥1 clock-hour ≤5% level | 88.4 | 89.2 | x |
| | | | | | | Average | 85.1 | 90 | 0.94 |
| | | | | | | Inferior quadrant | 86 | 90 | 0.93 |
| | | | | SD Cirrus HD-OCT | RNFL: clock-hour, quadrant and average | ≥1 clock-hour ≤5% level | 93.4 | 83.3 | x |
| | | | | | | Average | 86.8 | 90 | 0.95 |
| | | | | | | Inferior quadrant | 86.8 | 90 | 0.95 |

**Table 5.** Continued

| Reference | Definition of Glaucoma | *N* of Cases | *N* of Controls | OCT Device | Parameter | Best Parameter(s) | % Sensitivity | % Specificity | AUC |
|---|---|---|---|---|---|---|---|---|---|
| Li et al.[15] | GON and/or GVFD | 6 | 204 | Stratus OCT | RNFL: global, superior and inferior average | ≥1 parameter <5% | 67 | 85 | x |
| | | | | | | ≥1 parameter <1% | 50 | 94 | x |
| | | | | | ONH | Cup diameter ≥1.16mm | 83.3 | 84.4 | 0.91 |
| Moreno-Montañés et al.[50] | GVFD + IOP >21 mm Hg | 86 | 130 | Stratus OCT | RNFL: average, quadrant and clock-hours | Global average | 68.9 | 86.7 | 0.83 |
| | | | | Cirrus OCT | RNFL: average, quadrant and clock-hours | Superior quadrant | 68.9 | 91.4 | 0.84 |
| Mwanza et al.[51] | GON + GVFD | 73 | 146 | Cirrus HD-OCT | RNFL: average, quadrant, clock-hours | Clock-hour lower temporal | x | x | 0.96 |
| | | | | | ONH parameters | Vertical rim thickness | x | x | 0.96 |
| Park and Park[52] | GON + GVFD | 146 | 84 | Cirrus HD-OCT | RNFL: average, quadrant, clock-hours and RNFL Area Index | RNFL Area Index | x | x | 0.99 |
| | | | | | | Inferior quadrant | x | x | 0.97 |
| Park and Park[53] | GON + GVFD | 144 | 65 | Spectralis SD-OCT | RNFL: average, quadrants, and 4 superior and inferior segments | Global average | 86 | >90 | 0.95 |
| | | | | | ONH: laminar thickness; mean of mid-superior, center and mid-inferior | NA | 89 | >90 | 0.98 |
| Seo et al.[45] | GON + GVFD | 84 | 122 | Spectralis SD-OCT | RNFL: average, quadrants and 6 sectors | Abnormality (<1%) in ≥1 sector | 85.7 | 95.1 | x |
| | | | | | PPAA: central 20° area, 30x25° scan | Number of different cells | x | x | 0.96 |
| Sihota et al.[54] | GON + GVFD + IOP >22 mm Hg | 61 | 160 | Stratus OCT-3 | RNFL: average and quadrant | Average | 89.4 | 80.3 | 0.91 |

RNFL thickness value of 8 × 8 cells, > cell to cell comparison between corresponding cells across the hemisphere (difference ≥30 μm). FD, Fourier-domain; FLV, total sum of statistically significant GCC volume loss divided by the GCC map area; GCC, ganglion cell complex; GCIPL, ganglion cell-inner plexiform layer; GVFD, glaucomatous visual field defect; HD, high definition; IRL, inner retinal layer; PPAA, posterior pole asymmetry analysis; RNFL Area Index, proportion of normal RNFL area (≥1% age-matched controls); SD, spectral-domain; TD, time-domain; VCDR, vertical-cup disc ratio; x, sensitivity/specificity/AUC is not available.

glaucoma (median MD was –6.5 dB) and in this group the macular region was affected in approximately half of the patients (Table 3; sensitivity for the mean RGCL thickness in the inferior half of the macular region 53.7%). This is in agreement with recent studies assessing the macula with perimetry in detail and underlines the importance of macula testing in glaucoma care,[38,39] something that has been abandoned with the adoption of 6 × 6 degree perimetric grids. Hood et al.[17] suggested that the RGCL in a specific part of the inferior macula associates with the region of the optic disc where most glaucomatous damage occurs; the macular vulnerability zone. In our study, we found a sensitivity of 46.3% for this macular area. Because thickness measurements for this specific area are not available for each OCT device, we calculated the AUC and sensitivity for "mean RGCL thickness in the inferior half of the macular region" and found a sensitivity that was at least as high as the sensitivity of the MVZ (53.7%; $P = 0.25$ compared to the sensitivity of 46.3% of the MVZ). Taking the pathophysiology of glaucoma into account by using the 4 and 11 bundle regions-of-interest approach did not improve performance. Presumably, the large intersubject variability in the retinal nerve fiber bundle trajectories might explain the poor performance of an approach based on the average trajectories.[19] We previously found that combined analysis of the RNFL and RGCL thicknesses allowed for analyzing smaller regions-of-interest.[27] This approach did not increase performance in the current analysis, probably because smaller regions-of-interest were less informative for other reasons, like the intersubject variability of the retinal anatomy mentioned above. Glaucomatous damage causes retinal gliosis,[40] which may mask RNFL thinning on OCT.[41]

Table 5 gives an overview of published literature regarding glaucoma screening with OCT. We included studies with information on AUC, and/or sensitivity and specificity and with more than 200 cases and healthy controls in total. Four nonpopulation-based studies investigated macular parameters, in various layers, being the GCC,[42] RNFL + RGCL + IPL,[43] RGCL + IPL,[44] and the RNFL.[45] These macular parameters had AUCs ranging from 0.87 to 0.96; the peripapillary RNFL and ONH parameters in these studies had AUCs varying from 0.78 to 0.99. Obviously, a comparison of these studies is hampered by heterogeneity of the applied glaucoma definitions (reference standards): three of four studies used a glaucoma definition based on visual field loss and GON. In contrast, our reference standard for calling a case glaucoma was based solely on visual field loss (GVFL), that is, on functional changes. This may have biased the results toward a lower agreement with OCT, a technique that measures structural changes. With a more strict glaucoma definition based on GON and GVFL, the sensitivity for mean RGCL thickness in the inferior half of the macular region increased from 53.7% to 70.0%, with an increase in AUC from 0.85 to 0.93 (Table 4), and again the macular region outperformed the peripapillary region (Table 4). Generally, the reported AUCs of other studies seem to surpass that of our study. However, our study is a population-based study and cannot be compared to clinical studies, with their selection bias, directly. In a clinical setting, perimetry is generally confined to those patients who have a suspected ONH appearance. This will induce a selection bias toward abnormal structure, favoring an imaging technique, like OCT. In our population-based setting, perimetry was performed in all subjects. Baskaran et al.[46] included 508 healthy controls from a population-based study, but they selected 184 glaucoma cases from an eye center, where glaucoma diagnosis was based on GON and corresponding visual field loss. Li et al.[15] included community-based volunteer subjects, including 204 healthy controls and six cases with definite glaucoma, which also was defined as visual field loss and GON. Their best parameter was the cup diameter (AUC, 0.91; 83% sensitivity at 84% specificity). Another study invited individuals randomly from two rural areas[14] and consisted of 129 healthy controls and only nine glaucoma cases. The inclusion criterion for being a case was glaucomatous changes of the optic disc. Their best AUC (0.99) was found for the parameter "≥1 peripapillary quadrant sectors below P1"; with 100% sensitivity at 96% specificity.

Although the sensitivity we found is lower than in these clinical case-control studies, it is relatively high compared to other imaging techniques used in population-based studies. In the Rotterdam Study, we found a sensitivity of 35% at 97.5% specificity for the best parameter of the HRT (linear cup-disc ratio adjusted for disc area)[10]; a similar modest HRT screening performance was found in the Tajimi and Blue Mountains Eye studies.[9,11] Another study investigated scanning laser polarimetry (GDx-VCC) and found a sensitivity of 25.6% at a specificity of 97.0% for the parameter with the highest AUC (0.89; nerve fiber indicator).[12]

The strength of this study is the large number of subjects. However, the number of cases is a limitation, a consequence of the population-based design. There were 41 cases, which is lower than most clinical studies in Table 5. At the beginning of our study, we scanned only the right eye and, therefore, we missed 15 cases with unilateral GVFL in the left eye. Another strength is the glaucoma reference standard, which is based on visual field loss only. This avoids a selection bias toward abnormal structure (see above). On the other hand, we have probably missed some glaucoma cases with small macular defects and cases with superficial defects, due to the course 6 × 6 degree grid in combination with the requirement of three contiguous abnormal test locations and the preselection with supra-threshold testing, respectively.

Analyzing a series of parameters bears the risk of chance findings. We tried to avoid this as much as possible by limiting the number of parameters and by focusing on parameters inspired by the anatomy and pathophysiology of glaucoma. In the ideal situation, an external validation is performed. Data for such a validation were not available. For that reason, we performed a cross-validation using a leave-one-out resampling. The resulting adjusted AUC (0.84) of our best parameter, the mean RGCL thickness in the inferior half of the macular region, was essentially equal to the unadjusted AUC (0.85), indicating an unbiased estimate.

Because of the limited number of cases, we did not analyze early, moderate, and severe cases separately. However, we did some exploratory analyses. Correctly identified cases had a lower perimetric threshold sensitivity in the central part of the visual field and a greater axial length compared to cases that were not identified. The difference in axial length could be a technical issue or a real influence of axial length on the pathophysiology of glaucoma.[47]

In conclusion, in this population-based study OCT uncovers abnormalities in the macular region in many cases with early and moderate glaucoma detected with perimetry. Retinal ganglion cell loss in the macular region is at least as common as peripapillary RNFL abnormalities. The OCT-derived regional thickness–based screening only leads to missing approximately half of all glaucoma cases with manifest visual field loss in our population.

## *Acknowledgments*

Presented at the annual meeting of the Netherlands Ophthalmological Society, Maastricht, The Netherlands, March 2014; and the annual meeting of the Association for Research in Vision and Ophthalmology, Orlando, Florida, United States, May 2014.

Supported by Stichting Lijf en Leven, Krimpen aan de Lek; MD Fonds, Utrecht; Rotterdamse Vereniging Blindenbelangen, Rotterdam; Stichting Oogfonds Nederland, Utrecht; Blindenpenning, Amsterdam; Blindenhulp, The Hague; Algemene Nederlandse Vereniging ter Voorkoming van Blindheid (ANVVB), Doorn; Landelijke Stichting voor Blinden en Slechtzienden, Utrecht; Swart van Essen, Rotterdam; Stichting Winckel-Sweep, Utrecht; Henkes Stichting, Rotterdam; Laméris Ootech BV, Nieuwegein; Medical Workshop, de Meern; Topcon Europe BV, Capelle aan de IJssel, all in The Netherlands, and Heidelberg Engineering, Dossenheim, Germany. Also supported by the NWO Graduate Programme 2010 BOO (022.002.023; HS), the National Institute of Health (Bethesda, MD, USA) Grants R01 EY019112 and R01 EY018853, Veterans Administration Grant I01 CX000119, and the Arnold and Mabel Beckman Initiative for Macular Research. The authors alone are responsible for the content and writing of the paper.

Disclosure: **H. Springelkamp**, None; **K. Lee**, None; **R.C.W. Wolfs**, None; **G.H.S. Buitendijk**, None; **W.D. Ramdas**, None; **A. Hofman**, None**; J.R. Vingerling**, None; C**.C.W. Klaver**, Topcon (F); M**.D. Abràmoff**, P; **N.M. Jansonius**, None

## *References*

1. Airaksinen PJ, Alanko HI. Effect of retinal nerve fibre loss on the optic nerve head configuration in early glaucoma. *Graefes Arch Clin Exp Ophthalmol*. 1983;220:193–196.
2. Nickells RW. Ganglion cell death in glaucoma: from mice to men. *Vet Ophthalmol*. 2007;1(suppl 10):88–94.
3. Schuman JS, Hee MR, Puliafito CA, et al. Quantification of nerve fiber layer thickness in normal and glaucomatous eyes using optical coherence tomography. *Arch Ophthalmol*. 1995; 113:586–596.
4. Rohrschneider K, Burk RO, Kruse FE, Volcke, HE. Reproducibility of the optic nerve head topography with a new laser tomographic scanning device. *Ophthalmology*. 1994;101: 1044–1049.
5. Dreher AW. Retinal laser ellipsometry: a new method for measuring the retinal nerve fibre layer thickness distribution? *Clin Vis Sci*. 1992;7:481–488.
6. Weinreb RN, Dreher AW, Coleman A, Quigley H, Shaw B, Reiter K. Histopathologic validation of Fourier-ellipsometry measurements of retinal nerve fiber layer thickness. *Arch Ophthalmol*. 1990;108:557–560.
7. Choplin NT, Lundy DC. The sensitivity and specificity of scanning laser polarimetry in the detection of glaucoma in a clinical setting. *Ophthalmology*. 2001;108:899–904.
8. Oddone F, Centofanti M, Iester M, et al. Sector-based analysis with the Heidelberg Retinal Tomograph 3 across disc sizes and glaucoma stages: a multicenter study. *Ophthalmology*. 2009; 116:1106–1111.
9. Healey PR, Lee AJ, Aung T, Wong TY, Mitchell P. Diagnostic accuracy of the Heidelberg Retina Tomograph for glaucoma a population-based assessment. *Ophthalmology*. 2010;117: 1667–1673.
10. Ramdas WD, Wolfs RC, Hofman A, de Jong PT, Vingerling JR, Jansonius NM. Heidelberg Retina Tomograph (HRT3) in population-based epidemiology: normative values and criteria for glaucomatous optic neuropathy. *Ophthalmic Epidemiol*. 2011;18:198–210.
11. Saito H, Tsutsumi T, Araie M, Tomidokoro A, Iwase A. Sensitivity and specificity of the Heidelberg Retina Tomograph II Version 3.0 in a population-based study: the Tajimi Study. *Ophthalmology*. 2009;116:1854–1861.
12. Toth M, Kothy P, Vargha P, Hollo G. Accuracy of combined GDx-VCC and matrix FDT in a glaucoma screening trial. *J Glaucoma*. 2007;16:462–470.
13. Huang D, Swanson EA, Lin CP, et al. Optical coherence tomography. *Science*. 1991;254:1178–1181.
14. Bengtsson B, Andersson S, Heijl A. Performance of time-domain and spectral-domain Optical Coherence Tomography for glaucoma screening. *Acta Ophthalmol*. 2012;90:310–315.
15. Li G, Fansi AK, Boivin JF, Joseph L, Harasymowycz P. Screening for glaucoma in high-risk populations using optical coherence tomography. *Ophthalmology*. 2010;117:453–461.
16. Garvin MK, Abramoff MD, Lee K, Niemeijer M, Sonka M, Kwon YH. 2-D pattern of nerve fiber bundles in glaucoma emerging from spectral-domain optical coherence tomography. *Invest Ophthalmol Vis Sci*. 2012;53:483–489.
17. Hood DC, Raza AS, de Moraes CG, Liebmann JM, Ritch R. Glaucomatous damage of the macula. *Prog Retin Eye Res*. 2013;32:1–21.
18. Jansonius NM, Nevalainen J, Selig B, et al. A mathematical description of nerve fiber bundle trajectories and their variability in the human retina. *Vision Res*. 2009;49:2157–2163.
19. Jansonius NM, Schiefer J, Nevalainen J, Paetzold J, Schiefer U. A mathematical model for describing the retinal nerve fiber bundle trajectories in the human eye: average course, variability, and influence of refraction, optic disc size and optic disc position. *Exp Eye Res*. 2012;105:70–78.
20. Lee K, Kwon YH, Garvin MK, Niemeijer M, Sonka M, Abramoff MD. Distribution of damage to the entire retinal ganglion cell pathway: quantified using spectral-domain optical coherence tomography analysis in patients with glaucoma. *Arch Ophthalmol*. 2012;130:1118–1126.
21. Hofman A, Darwish Murad S, van Duijn CM, et al. The Rotterdam Study: 2014 objectives and design update. *Eur J Epidemiol*. 2013;28:889–926.
22. Wolfs RC, Borger PH, Ramrattan RS, et al. Changing views on open-angle glaucoma: definitions and prevalences–The Rotterdam Study. *Invest Ophthalmol Vis Sci*. 2000;41:3309–3321.
23. Czudowska MA, Ramdas WD, Wolfs RS, et al. Incidence of glaucomatous visual field loss: a ten-year follow-up from the Rotterdam Study. *Ophthalmology*. 2010;117:1705–1712.
24. Garvin, MK et al. Intraretinal layer segmentation of macular optical coherence tomography images using optimal 3-D graph search. *IEEE Trans Med Imaging*. 2008;27:1495–1505.
25. Garvin MK, Abramoff MD, Kardon R, Russell SR, Wu X, Sonka M. Automated 3-D intraretinal layer segmentation of macular spectral-domain optical coherence tomography images. *IEEE Trans Med Imaging*. 2009;28:1436–1447.
26. Lee K, Neimeijer M, Garvin MK, Kwon YH, Sonka M, Abramoff MD. Segmentation of the optic disc in 3-D OCT scans of the optic nerve head. *IEEE Trans Med Imaging*. 2010;29:159–168.
27. Springelkamp H, Lee K, Ramdas WD, et al. Optimizing the information yield of 3-D OCT in glaucoma. *Invest Ophthalmol Vis Sci*. 2012;53:8162–8171.
28. DeLong ER, DeLong DM, Clarke-Pearson DL. Comparing the areas under two or more correlated receiver operating characteristic curves: a nonparametric approach. *Biometrics*. 1988;44:837–845.
29. Ramdas WD, Rizopoulos D, Wolfs RC, et al. Defining glaucomatous optic neuropathy from a continuous measure of optic nerve damage - the optimal cut-off point for risk-factor analysis in population-based epidemiology. *Ophthalmic Epidemiol*. 2011;18:211–216.
30. Inuzuka H, Kawase K, Sawada A, Aoyama Y, Yamamoto T. Macular ganglion cell complex thickness in glaucoma with superior or inferior visual hemifield defects. *J Glaucoma*. 2013;22:60–64.
31. Kimura Y, Hangai M, Matsumoto A, et al. Macular structure parameters as an automated indicator of paracentral scotoma in early glaucoma. *Am J Ophthalmol*. 2013;156:907–917.
32. Na JH, Lee K, Lee JR, Baek S, Yoo SJ, Kook MS. Detection of macular ganglion cell loss in preperimetric glaucoma patients with localized retinal nerve fibre defects by spectral-domain

Investigative Ophthalmology & Visual Science

optical coherence tomography. *Clin Experiment Ophthalmol*. 2013;41:870–880.

33. Nouri-Mahdavi K, Nowroozizadeh S, Nassiri N, et al. Macular ganglion cell/inner plexiform layer measurements by spectral domain optical coherence tomography for detection of early glaucoma and comparison to retinal nerve fiber layer measurements. *Am J Ophthalmol*. 2013;156:1297–1307.
34. Rao HL, Zangwill LM, Weinreb RN, Sample PA, Alencar LM, Medeiros FA. Comparison of different spectral domain optical coherence tomography scanning areas for glaucoma diagnosis. *Ophthalmology*. 2010;117:1692–1699.
35. Tan O, Chopra V, Lu AT, et al. Detection of macular ganglion cell loss in glaucoma by Fourier-domain optical coherence tomography. *Ophthalmology*. 2009;116:2305–2314.
36. Tan O, Li G, Lu AT, et al. Mapping of macular substructures with optical coherence tomography for glaucoma diagnosis. *Ophthalmology*. 2008;115:949–956.
37. Wang M, Lu AT, Varma R, et al. Combining information from 3 anatomic regions in the diagnosis of glaucoma with time-domain optical coherence tomography. *J Glaucoma*. 2014;23:129–135.
38. Hood DC, Raza AS, de Moraes CG, et al. Initial arcuate defects within the central 10 degrees in glaucoma. *Invest Ophthalmol Vis Sci*. 2011;52:940–946.
39. Schiefer U, Papagiorgiou E, Sample PA, et al. Spatial pattern of glaucomatous visual field loss obtained with regionally condensed stimulus arrangements. *Invest Ophthalmol Vis Sci*. 2010;51:5685–5689.
40. Wang L, Cioffi GA, Cull G, Dong J, Fortune B. Immunohistologic evidence for retinal glial cell changes in human glaucoma. *Invest Ophthalmol Vis Sci*. 2002;43:1088–1094.
41. Grieshaber MC, Moramarco F, Schoetzau A, Flammer J, Orguel S. Detection of retinal glial cell activation in glaucoma by time domain optical coherence tomography. *Klin Monbl Augenheilkd*. 2012;229:314–318.
42. Garas A, Vargha P, Hollo G. Diagnostic accuracy of nerve fibre layer, macular thickness and optic disc measurements made with the RTVue-100 optical coherence tomograph to detect glaucoma. *Eye (Lond)*. 2011;25:57–65.
43. Huang JY, Pekmezci M, Mesiwala N, Kao A, Lin S. Diagnostic power of optic disc morphology, peripapillary retinal nerve fiber layer thickness, and macular inner retinal layer thickness in glaucoma diagnosis with fourier-domain optical coherence tomography. *J Glaucoma*. 2011;20:87–94.
44. Jeoung JW, Choi YJ, Park KH, Kim DM. Macular ganglion cell imaging study: glaucoma diagnostic accuracy of spectral-domain optical coherence tomography. *Invest Ophthalmol Vis Sci*. 2013;54:4422–4429.
45. Seo JH, Kim TW, Weinreb RN, Park KH, Kim SH, Kim DM. Detection of localized retinal nerve fiber layer defects with posterior pole asymmetry analysis of spectral domain optical coherence tomography. *Invest Ophthalmol Vis Sci*. 2012;53:4347–4353.
46. Baskaran M, Ong EL, Li JL, et al. Classification algorithms enhance the discrimination of glaucoma from normal eyes using high-definition optical coherence tomography. *Invest Ophthalmol Vis Sci*. 2012;53:2314–2320.
47. Marcus MW, de Vries MM, Junoy Montolio FG, Jansonius NM. Myopia as a risk factor for open-angle glaucoma: a systematic review and meta-analysis. *Ophthalmology*. 2011;118:1989–1994.
48. Bowd C, Hao J, Tavares IM, et al. Bayesian machine learning classifiers for combining structural and functional measurements to classify healthy and glaucomatous eyes. *Invest Ophthalmol Vis Sci*. 2008;49:945–953.
49. Leung CK, Lam S, Weinreb RN, et al. Retinal nerve fiber layer imaging with spectral-domain optical coherence tomography: analysis of the retinal nerve fiber layer map for glaucoma detection. *Ophthalmology*. 2010;117:1684–1691.
50. Moreno-Montanes J, Olmo N, Alvarez A, Garcia N, Zarranz-Ventura J. Cirrus high-definition optical coherence tomography compared with Stratus optical coherence tomography in glaucoma diagnosis. *Invest Ophthalmol Vis Sci*. 2010;51:335–343.
51. Mwanza JC, Oakley JD, Budenz DL, Anderson DR, Cirrus Optical Coherence Tomography Normative Database Study Group. Ability of cirrus HD-OCT optic nerve head parameters to discriminate normal from glaucomatous eyes. *Ophthalmology*. 2011;118:241–248.
52. Park HY, Park CK. Structure-function relationship and diagnostic value of RNFL Area Index compared with circumpapillary RNFL thickness by spectral-domain OCT. *J Glaucoma*. 2013;22:88–97.
53. Park HY, Park CK. Diagnostic capability of lamina cribrosa thickness by enhanced depth imaging and factors affecting thickness in patients with glaucoma. *Ophthalmology*. 2013;120:745–752.
54. Sihota R, Sony P, Gupta V, Dada T, Singh R. Diagnostic capability of optical coherence tomography in evaluating the degree of glaucomatous retinal nerve fiber damage. *Invest Ophthalmol Vis Sci*. 2006;47:2006–2010.

Investigative Ophthalmology & Visual Science